On the mechanical aspect of additive manufactured polyether-ether-ketone scaffold for repair of large bone defects

Seyed Ataollah Naghavi[1,#], Changning Sun[2,#], Mahbubeh Hejazi[3], Maryam Tamaddon[1], Jibao Zheng[2], Leilei Wang[2], Chenrui Zhang[2], Swastina Nath Varma[1], Dichen Li[2], Mehran Moazen[3], Ling Wang[2,], Chaozong Liu[1,*]*

Key Words:
additive manufacturing; bone scaffold; finite element analysis; mechanical behaviour; lattice structure; PEEK scaffold

From the Contents

ABSTRACT

Polyether-ether-ketone (PEEK) is widely used in producing prosthesis and have gained great attention for repair of large bone defect in recent years with the development of additive manufacturing. This is due to its excellent biocompatibility, good heat and chemical stability and similar mechanical properties which mimics natural bone. In this study, three replicates of rectilinear scaffolds were designed for compression, tension, three-point bending and torsion test with unit cell size of 0.8 mm, a pore size of 0.4 mm, strut thickness of 0.4 mm and nominal porosity of 50%. Stress-strain graphs were developed from experimental and finite element analysis models. Experimental Young's modulus and yield strength of the scaffolds were measured from the slop of the stress-strain graph to be 395 and 19.50 MPa respectively for compression, 427 and 6.96 MPa respectively for tension, 257 and 25.30 MPa respectively for three-point bending and 231 and 12.83 MPa respectively for torsion test. The finite element model was found to be in good agreement with the experimental results. Ductile fracture of the struct subjected to tensile strain was the main failure mode of the PEEK scaffold, which stems from the low crystallinity of additive manufacturing PEEK. The mechanical properties of porous PEEK are close to those of cancellous bone and thus are expected to be used in additive manufacturing PEEK bone implants in the future, but the lower yield strength poses a design challenge.

http://doi.org/10.12336/biomatertransl.2022.02.006

How to cite this article:
Naghavi, S. A.; Sun, C.; Hejazi, M.; Tamaddon, M.; Zheng, J.; Wang, L.; Zhang, C.; Varma, S. N.; Li, D.; Moazen, D.; Wang, L.; Liu, C. On the mechanical aspect of additive manufactured polyether-ether-ketone scaffold for repair of large bone defects. *Biomater Transl.* **2022**, *3*(2), 142-151.

Introduction

Polyether-ether-ketone (PEEK) is an aromatic polymer with one ketone and two ether bonds in the molecular backbone with a chemical formula of poly (oxy-1, 4-phenyleneoxy-1, 4-phenylenecarbonyl-1, 4-phenylene). PEEK is a semi-crystalline, high-performance thermoplastic, which was firstly synthesized in 1978.[1-3] The multiple benzene rings in the molecular chain of PEEK provide heat resistance and chemical stability, and the two ether bonds and a carbanyl group provide good flexibility, giving PEEK excellent heat, wear, chemical and radiation resistance. As a biomaterial, the good resistance and stability of PEEK allow it to be implanted into human body and stay for a long period. In terms of mechanical properties, the density (1.28–1.32 g/mm^3), elastic modulus (3 GPa) and yield stress (110 MPa)[4] are closer to those of human bone compared to biomedical metal materials such as titanium-based alloys, cobalt-based alloys and stainless steel, effectively reducing the stress shielding with sufficient load-bearing capacity. PEEK is radiolucent so that there are no artefacts on X-rays which can be detrimental to post-operative examination. With these advantages, PEEK has emerged as the promising biomaterial for the reconstruction of bone defects.[2, 5]

With the development of precision medicine, customized repair of bone defect is becoming increasingly important. Additive manufacturing (AM), which is common known as three-

dimensional (3D) printing, is a fully digitally driven manufacturing method that build parts layer-by-layer through the forming of powder, filament or liquid materials into solid structures.[6] The new forming principle allows AM to integrate manufacturing parts with complex macro and micro structures. Thus AM is particularly suitable for the manufacture of customized implant with both complex geometry matching with the anatomy of human body and micro-structures which offers long-term stability leading by bone ingrowth into the porous structure.[7] To data, AM implant with porous structure has become a main technique for personalised bone repair.

Additive manufactured PEEK orthopaedic implant has been studied in recent years and has been used in clinical practices. Kang et al. [8] reported the first AM PEEK rib prosthesis in 2018 in which fused filament fabrication (FFF), which was also known as fused deposition modelling, was used to manufacture the PEEK rib prosthesis. The mechanical properties of the PEEK rib prosthesis were proved to be better than that of the human natural rib. FFF is a filament-based AM technology, as shown in **Figure 1**. The filament is made using screw extruder and is fed into the heated nozzle of the AM machine, where the filament is melted and extruded from the nozzle onto the substrate. By this means, a part was manufactured layer by layer. A series of clinical cases of PEEK prostheses used in the reconstruction of chest wall defects were then reported by Wang et al.,[9] the clinical trial showed the safety and effectiveness of AM PEEK prosthesis. Similar techniques have been used in the clinical application of mandibular prosthesis,[10] scapula replacement[11] and removable dental prosthesis.[12] Whereas these implants were commonly located in the trunk of human body, they were fewer clinical reports of PEEK implant for reconstruction of lower limbs, probably due to the doubt about the strength of PEEK material. A PEEK femoral segment made by FFF was employed to reconstruct the removed femoral segment eroded by tumour,[13] but a metal intramedullary nail was inserted into the PEEK prosthesis as the load-bearing enhancement. To authors' knowledge, there was few published paper that reported the AM PEEK porous orthopaedic implants, which, however, was believed to be an effective way of improving the osseointegration of PEEK.[14, 15] The research of Zheng et al. [16] and Zhu et al.[17] have reported that the AM PEEK scaffolds with controllable pore size facilitated the bone ingrowth and osseointegration. Nevertheless, porous structure compromises the overall mechanical properties of PEEK implant. The mechanical property of the porous PEEK implants is an important aspect that regulates the *in vivo* performance of the implants. An in-depth understanding of mechanical behaviour and failure modes of AM PEEK porous structures under different loading patterns is essential for the clinical translation of AM PEEK implants. In the existing studies, compressive properties of PEEK and PEEK-based composite porous structures were investigated,[18-20] while other loading patterns such as tension, bending and torsion were barely studied. Understanding the compressive properties of PEEK porous structures is not sufficient when bone implants are subjected to complex loading in the human body, and it is therefore important that the mechanical behaviour of PEEK porous structures is investigated systematically and comprehensively, which will provide the basis for the clinical translation of AM PEEK porous implants.

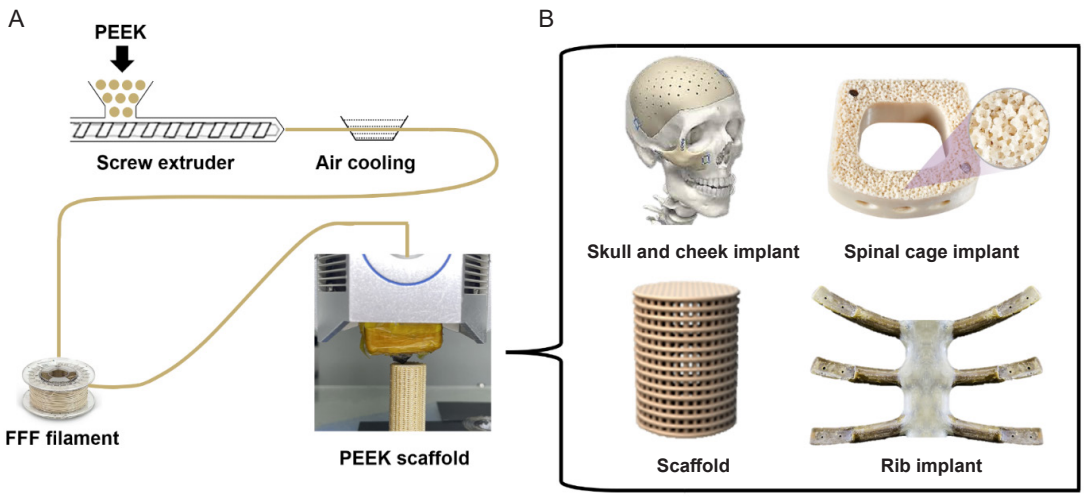

Figure 1. (A, B) Schematic illustration of the three-dimensional printing process of PEEK (A) and example application of PEEK material in biomedical field (B). FFF: fused filament fabrication; PEEK: polyether-ether-ketone.

***Corresponding authors:**
Ling Wang, menlwang@mail.xjtu.edu.cn; Chaozong Liu, chaozong.liu@ucl.ac.uk.

#Author Equally.

1 Institute of Orthopaedic & Musculoskeletal Science, University College London, Royal National Orthopaedic Hospital, London, UK; 2 State Key Laboratory for Manufacturing Systems Engineering, School of Mechanical Engineering, Xi'an Jiaotong University, Xi'an, Shaanxi Province, China; 3 Department of Mechanical Engineering, University College London, London, UK.

In this study, the mechanical properties of AM PEEK porous structure were systematically investigated. Porous samples for tension, bending, compression and torsion with orthogonal structure were manufactured by FFF to investigate the mechanical properties as well as the failure modes of PEEK porous structure under different loading patterns. This study provides a bridge for the design, manufacturing and clinical translation of PEEK orthopaedic implants from the perspective of mechanics.

Methods

Polyether-ether-ketone scaffold

For a comprehensive understanding of the mechanical properties of porous structures of AM PEEK, porous specimens for compression, tension, three-point bending and torsion test were designed. The geometry and sizes of the test specimens are shown in **Figure 2**. All scaffolds were built by the same orthogonal structure with a unit cell size of 0.8 mm, a pore size of 0.4 mm and a struct size of 0.4 mm, thus the porous part of the scaffolds had a nominal porosity of 50%.

A commercial PEEK raw material (450G, VICTREX, Rotherham, UK) with weight-average a molecular weight of approximately 37,000[21] was involved in this investigation. PEEK filament with a diameter of 1.75 mm was made by a twin-screw extruder. All the samples were manufactured by a commercial 3D printer (Engineer 200, Jugao AM, Xi'an, China) through FFF technology, which was also known as fused deposition modelling. The parameters of the 3D printing processes were summarized in **Table 1**.

Morphological and mechanical characterizations

TThe fabricated PEEK samples were scanned and their morphology was characterized using a Nikon XTH 225 ST micro-computed tomography (micro-CT; New York, NY, USA). The scans were performed with a tube voltage of 102 kV, tube current of 96 μA, a scan time of 30 minutes and a voxel size of 10 μm × 10 μm × 10 μm. Each sample was rotated from 0° to 180° in steps of 0.5° and three images were recorded to obtain an average radiograph image. Micro-CT data were then reconstructed into two-dimensional slices, representing the cross-sectional images of the scaffolds with a commercial software package (VGSTUDIO MAX 2.2.6, Volume Graphics, Heidelberg, Germany). The reconstruction process includes ring artifact reduction of 8, beam hardening correction of 25%, and lower and upper histogram ranges of 0 and 0.13, respectively. Pore size, strut thickness, porosity, surface area and scaffold volume were measured using CTAn software package (CTAn, Skyscan N.V., Kontich, Belgium). Pore size and strut thickness were measured at 15 different locations in five different slices. Hence, there were 75 pore size and 75 strut thickness measurements.

Mechanical properties of the PEEK samples were obtained by testing three bulk compression samples (10 mm × 20 mm) and three dogbone tension samples using an Instron mechanical testing machine (model 5969, 50 kN load cell, Instron, Norwood, MA, USA). Bluehill® Universal software (version 2016; Instron) was used to control the machine and record the respective load-displacement measurements at 10 Hz. Bulk compression samples were placed between two flat aluminum

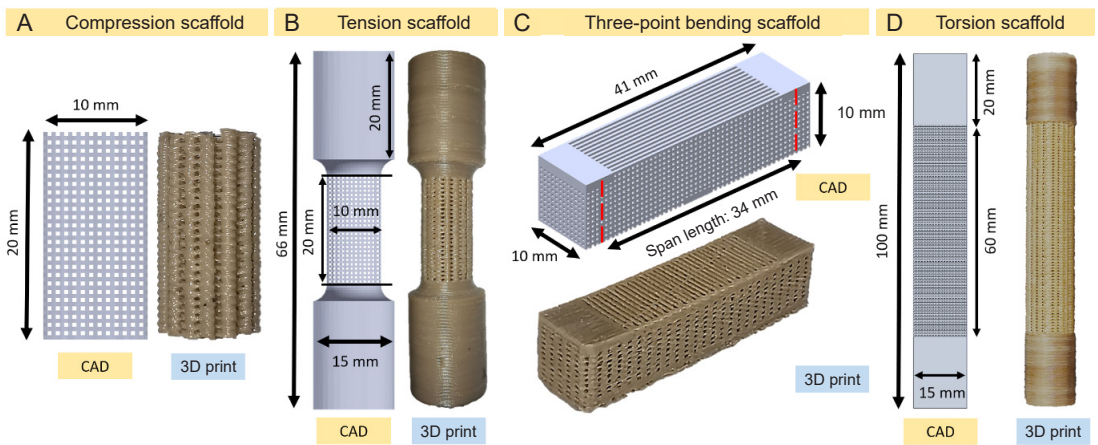

Figure 2. (A–D) Schematic CAD design and AM manufactured test specimens for compression (A), tension (B), three-point bending test (C), and torsion (D). 3D: three-dimensional; AM: additive manufacturing; CAD: computer-aided design.

Table 1. The process parameters of three-dimensional printing

Parameter	Value
Nozzle temperature (°C)	420
Ambient temperature (°C)	20
Nozzle diameter (mm)	0.4
Printing speed (mm/s)	20
Layer thickness (mm)	0.2

platens and only vertical movement was allowed. The bulk columns were compressed with a constant strain rate of 0.01 mm/s until failure. Dogbone tension samples were fixed with a grip length of 20 mm and were in tension with a constant strain rate of 0.01 mm/s until failure.

Similar to the bulk compression samples, compression scaffolds were also placed between two flat aluminum platens and only vertical movement was allowed. The scaffolds were compressed with a constant crosshead displacement of 0.01 mm/s to 25% strain to estimate the yield strength (σ_y). Compression tests were all according to ISO 13314:2011.[22] The same ISO standard was used to determine the stiffness (E) and yield strength (σ_y) from the obtained stress-strain curve. Stiffness was measured as the maximum slope of the elastic region of the stress-strain curve. Yield strength (σ_y) was computed by intersecting the stress-strain curve with a 0.2% offset line parallel to the elastic region.

E is calculated as follows:

$$E = \frac{\sigma}{\varepsilon} = \frac{\frac{F}{A}}{\frac{\Delta L}{L}} \quad (1)$$

Where is the stress, F is the vertical reaction force, A is the initial cross-sectional area of the upper surface of the scaffold, ε is the strain, ΔL is the displacement of the upper surface in the vertical direction, and L is the initial length of the scaffold.

Diameter of the round porous tensile samples was set to be at least 12.5 times the unit cell size of the lattice structure with parallel length to diameter ratio of at least 2:1 (10 mm × 20 mm). The samples were gripped over a 20 mm length on either side. Tensile testing was conducted with a crosshead displacement of 0.01 mm/s until failure. The strain was calculated as the measured displacement divided by the specimen's initial parallel length, while stress (σ) was calculated as the measured load (F) divided by the specimen's initial cross-sectional area. Young's modulus (E) and tensile yield strength (σ_y) (0.2% offset of the linear regression of the initial loading) of the scaffolds were measured from the stress-strain graphs.

Porous three-point bending PEEK samples were tested with a crosshead displacement of 0.005 mm/s until failure. Bending strain (ε) was the measured displacement divided by the specimen's initial thickness (d) and bending stress (σ) was measured as follows:

$$\text{Bending stress } (\sigma) = \frac{3FL_S}{2bd^2} \quad (2)$$

Where F is the vertical reaction force, L_S is the span length, b is the width and d is the thickness of the bending scaffold. Bending modules (E_f) and bending strength (σ_f) (0.2% offset of the linear regression of the initial loading) of the scaffolds were measured from the bending stress-strain graphs.

Torsion samples were designed and tested according to ASTM E143–13.[23] The diameter of the round porous torsion samples was set to be at least five times the unit cell size of the lattice structure with a gauge length to diameter ratio of at least 4:1. Torsional testing was conducted using a MTS 858 machine (MTS, Eden Prairie, MN, USA) under quasi-static conditions. Torsion samples were placed between two v-jaws and only torsional movement was allowed. Each test was conducted at a constant speed of 30°/min (which is high enough to make creep negligible) until failure. Torsion samples had a diameter of 15 mm and a gauge length (L) of 60 mm and a total length of 100 mm. The top and bottom grip sections of the sample were each 20 mm and were long enough to be attached to the machine grips. Torque (T) (N·mm) and angle of twist (θ) (rad) were measured at 10 Hz and are used to calculate the shear stress (τ) and shear strain (γ) as shown below:

$$\text{Shear stress } (\tau) = \frac{Tr}{J} \quad (3)$$

$$\text{Shear strain } (\gamma) = \frac{\theta r}{L} \quad (4)$$

Where J is the polar moment of inertia of solid bar (mm^4) and r is the radius (mm) of the bar. The polar moment of inertia of the scaffold was calculated from the smallest cross-sectional area of the scaffolds with a built-in block of nTopology software (version 3.25.3, nTopology Inc., New York, NY, USA). Torsional stiffness and torsional strength (0.2% offset of the linear regression of the initial loading) of the scaffolds were measured from the torsional stress-strain graphs.

Finite element analysis

Finite element (FE) analysis (FEA) was performed on rectilinear scaffolds in compression, tension and three-point bending test. These scaffolds are generated on Solidworks software (version 2021, Solid-Works Corp., Dassault Systemes, Concord, MA, USA) and are exported as parasolid file to be imported nTopology software where we can define FE mesh to the scaffolds. FE mesh files are then imported to Abaqus software (version 2019, Dassault Systèmes Simulia Corp., Johnston, RI, USA) to perform the FEA study. Previously it has been shown by Maskery et al.[24] that the unit cell repeat of a minimum of 4 × 4 × 4 unit cell is needed in every direction which can effectively eliminate the size effect on the structural performance of the unit cell. Therefore, the results of this study can be applied to larger structures such as large bone effects. For FEA compression and tension scaffold samples, we have 12.5-unit cells in diameter and 25-unit cells in height. For three-point bending scaffold samples, we have 51-unit cells in length, 12.5-unit cells in height and 12.5-unit cells in width. For torsion scaffold samples, we have 18.75-unit cells in diameter and 75-unit cells in height. Mesh convergence analysis was carried out on rectilinear scaffold with tetrahedral elements (C3D10) from element size of 0.05 mm up to 2 mm and it was shown that the results were converged within 5% when element size is 0.1 mm. The compression, tension, three-point bending and torsion scaffolds converged with about 10, 10.2, 10.2 and 44.3 million elements.

To model the FE scaffolds, a general static step was used. The FE model of compression, tension and three-point bending scaffolds were loaded uniaxially in compression and tension with the following boundary conditions. For compression and tensile testing, two rigid circular plates were created. The nodes at the bottom and top faces of the scaffolds were tied (fixed) to the bottom and top plates in all directions respectively. The bottom plate was fixed (Encastre) in all directions and a reference point was introduced and constrained to the center of

the top plate which was allowed to move in a uniaxial direction. This reference point would allow us to apply a uniform uniaxial displacement to all the top nodes of the scaffold and eventually deform the lattice structure until it yields. For compression testing, a vertical displacement of 3 mm on the reference point in the negative Y direction was applied with a constant strain rate of 0.1 s^{-1}. For tension testing, a vertical displacement of 3 mm on the reference point in the positive Y direction was applied with a constant strain rate of 0.1 s^{-1}. The respective reaction force (F) was then measured from this single reference point node and as a result, compressive and tensile Young's modulus (E) and yield strength (σ_y) (0.2% offset of the linear regression of the initial loading) of the scaffolds were measured from the obtained stress-strain graphs.

For three-point bending, two semicircle supports and a semicircle loader with a 5 mm radius were created. To allow sliding between the model and the supports, a coefficient of friction (0.2) was introduced with hard contact. A reference point was defined on the top surface of the semicircle loader and a vertical displacement of 3.5 mm on the reference point in the negative Y direction was applied with a constant strain rate of 0.1 s^{-1}. The respective reaction force (F) was then measured from this single reference point node. Hence, bending modules (E_f) and bending strength (σ_f) (0.2% offset of the linear regression of the initial loading) of the scaffolds were measured from the bending stress-strain graphs.

For the torsion test, the bottom grip section of the model was fixed (Encastre) in all directions and the top grip section was coupled to a reference point on the top surface of the model. A moment of 4500 N·mm was applied to the reference point and the respective twist (rad) was measured from this single reference point node. As a result, torsional stiffness and torsional strength (0.2% offset of the linear regression of the initial loading) of the scaffolds were measured from the torsional stress-strain graphs.

Obtained results of a FE model can vary significantly based on the input material properties of the model. Hence, to carefully input these materials' properties into Abaqus, data of stress-strain curve from the solid dogbone tensile sample were obtained. Tensile Young's modulus, yield strength (σ_y) (0.2% offset) and plastic strain-stress data were recorded and used to model the elastic and plastic material properties of the lattice structures. The loading plates in compression testing were assumed to be rigid; as such, the material properties are irrelevant. The PEEK bulk material was assumed to be solid and homogeneous. The Poisson's ratio was set as 0.3. Isotropic elasticity and isotropic plastic hardening models were used in all the simulations.

Results

Morphological examination: designed vs. manufactured

Important morphological characteristics such as pore size, porosity, strut thickness and surface to volume of the manufactured samples were characterized and measured by micro-CT and were compared to their designed CAD values. **Table 2** shows the morphological comparison results of micro-CT and CAD values for rectilinear scaffold. The results show that the averaged measured strut thicknesses (0.31 ± 0.01 μm) are thinner than the designed value of 0.4 mm and have a percentage error of approximately 22% between the two values. This is due to the struts shrinkage after printing and getting fully solid. Indeed, this shrinkage in strut thickness results in a larger pore size of the printed scaffolds. The averaged measured pore size (0.46 ± 0.03 μm) is thicker than the designed value of 0.4 mm and has a percentage error of approximately 15% between the two values. This reduction of strut thickness and increase in pore size resulted in a higher porosity (61%) than the designed porosity (50%). Surface to volume ratio of the printed scaffold was also measured to be 8.08 mm^{-1} which is larger by less than 7% compared to the designed scaffold (7.56 mm^{-1}). **Figure 3** shows the visual comparison of strut thickness and pore size of the designed and printed scaffolds in horizontal and vertical planes.

Experimental mechanical behaviour

Bulk compression and tension

Figure 4 shows the experimental results of bulk column compression and dogbone tension PEEK samples. At first sight, it is clear that the compressive Young's modulus (1.58 ± 0.06 GPa) is slightly (8%) lower than the tensile Young's modulus (1.71 ± 0.07 GPa), whereas the compressive yield strength (62.00 ± 1.26 MPa) is slightly (3%) higher than the tensile yield strength (60.00 ± 0.37 MPa).

Scaffold compression, tension, three-point bending and torsion

Rectilinear scaffolds were tested experimentally under compression, tension, three-point bending and torsion. **Figure 5** shows the experimental setup of these four experiments with their respective micro-CT scan images. Compression scaffold had an average Young's modulus and yield strength of 395 ± 45 MPa and 19.50 ± 0.64 MPa respectively. Tension scaffold had an average Young's modulus and yield strength of 427 ± 11 MPa and 6.96 ± 0.80 MPa respectively. Three-point bending

Table 2. Comparison of morphological properties of CAD data and micro-CT data

	CAD	Micro-CT	% Error
Porosity (%)	50	61.05±0.86	22.1
Strut thickness (mm)	0.4	0.31±0.01	22.5
Pore size (mm)	0.4	0.46±0.03	15.0
Surface to volume ratio (mm^{-1})	7.56	8.08±0.24	6.9

Note: CAD: computer aided design; micro-CT: micro-computed tomography.

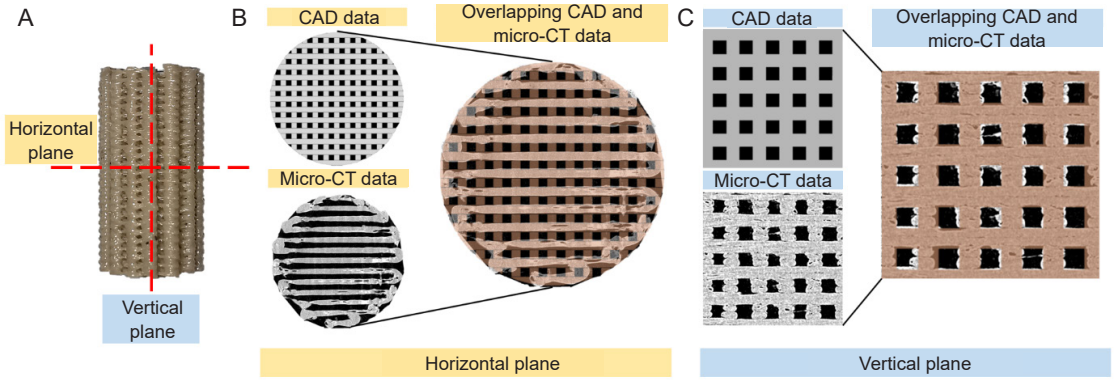

Figure 3. (A) Compression scaffold with defined horizontal and vertical planes (red dotted lines). (B, C) Overlapping CAD data and micro-CT data in horizontal (B) and vertical planes (C). CAD: computer aided design; micro-CT: micro-computed tomography.

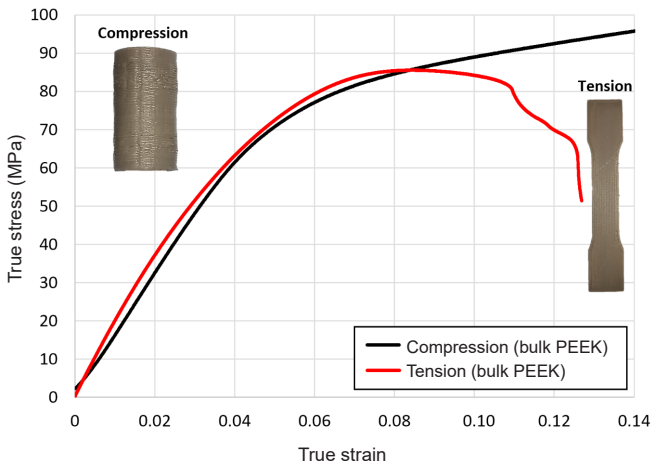

Figure 4. Compression and tension behaviour of bulk additively manufactured PEEK. PEEK: polyether-ether-ketone.

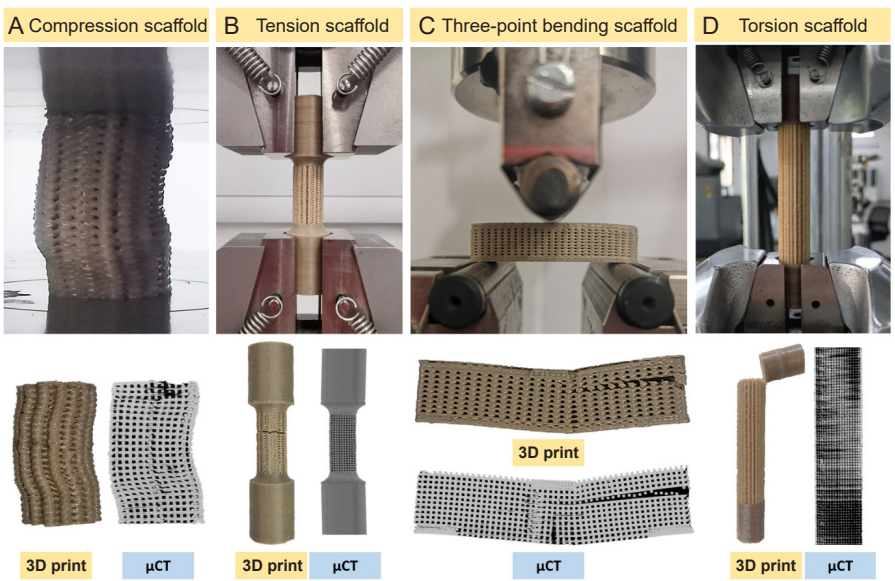

Figure 5. (A–D) Corresponding experimental mechanical testing images of compression (A), tension (B), three-point bending (C) and torsion (D) scaffolds. 3D: three-dimensional; µCT: micro-computed tomography.

scaffold had an average Young's modulus and yield strength of 257 ± 10 MPa and 25.30 ± 0.44 MPa respectively. Torsion scaffold had an average Young's modulus and yield strength of 231 ± 10 MPa and 12.83 ± 0.60 MPa respectively. Similar to bulk column compression and dogbone tension PEEK samples, scaffold compressive Young's modulus is slightly lower (8%) than the tensile young's modulus, whereas the compressive yield strength is significantly (2.8×) higher than the tensile yield strength. It is interesting that the ratio of tensile to compressive Young's modulus of bulk and scaffold are almost the same at 8%. **Figure 6** shows the stress-strain of the experimental tests under compression, tension, three-point bending and torsion. It is interesting that the ratio of tensile to compressive Young's modulus of bulk and scaffold are almost the same at 8%. **Figure 6** shows the stress-strain of the experimental tests under compression, tension, three-point bending and torsion. The ratio of strain of the experimental tests under compression, tension, three-point bending and torsion.

Finite element analysis mechanical behaviour

FEA was performed for respectively designed compression, tension, three-point bending and torsion scaffolds. Stress-strain graph of each test was developed. Compressive stiffness was obtained from the maximum slope in the linear elastic region and yield strength was measured from 0.2% offset of the linear regression of the initial loading. Compression scaffold had Young's modulus and yield strength of 527 MPa and 18.72 MPa respectively. Tension scaffold had a Young's modulus and yield strength of 437 MPa and 16 respectively. Three-point bending scaffold had Young's modulus and yield strength of 240 MPa and 32.74 MPa respectively. Torsion scaffold had a Young's modulus and yield strength of 305 MPa and 17.72 MPa respectively. **Figure 6** illustrates the stress-strain of the FEA tests under compression, tension, three-point bending and torsion. Comparing compression and tension FEA results, compression scaffold has a 20% higher Young's modulus and 1.2% higher yield strength than tension scaffold. **Figure 7** shows the section view of the FEA results when loaded in compression (**Figure 7A**), tension (**Figure 7B**), three-point bending (**Figure 7C**) and torsion (**Figure 7D**), which shows a smooth transition of forces from the vertical structs to the horizontal struts in all cases. By applying a displacement of 3 mm to the compression and tension sample, a maximum stress of 102 MPa was observed. This suggests that the scaffold should have reached the expected yield strength of the experimental compression (19.50 ± 0.64 MPa) and tension (6.96 ± 0.8 MPa) scaffolds. When 3.5 mm displacement was applied to the bending FE model, a maximum stress of 356 was observed which was well above the yield strength of the experimental bending scaffold (25.30 ± 0.44 MPa). In torsion sample, a moment of 5000 N·mm was applied and a maximum stress of 87.5 MPa was observed.

Failure mechanisms and failure model

Figure 8 illustrates the digital microscope images of the cracked tensile (**Figure 8A**) and bending (**Figure 8B**) scaffolds. As it can be seen, the strut has been elongated slightly before a sudden fracture occurs. This is called a ductile fracture mode. The characteristics of ductile fracture were also observed in the stress-strain curves of the compression, tension and three-point bending experiments (**Figure 6A–C**), where the compression and bending loading have the following characteristic stages: elastic regime, yielding, post-yielding, and plateau. The ambient temperature was set to 20 during

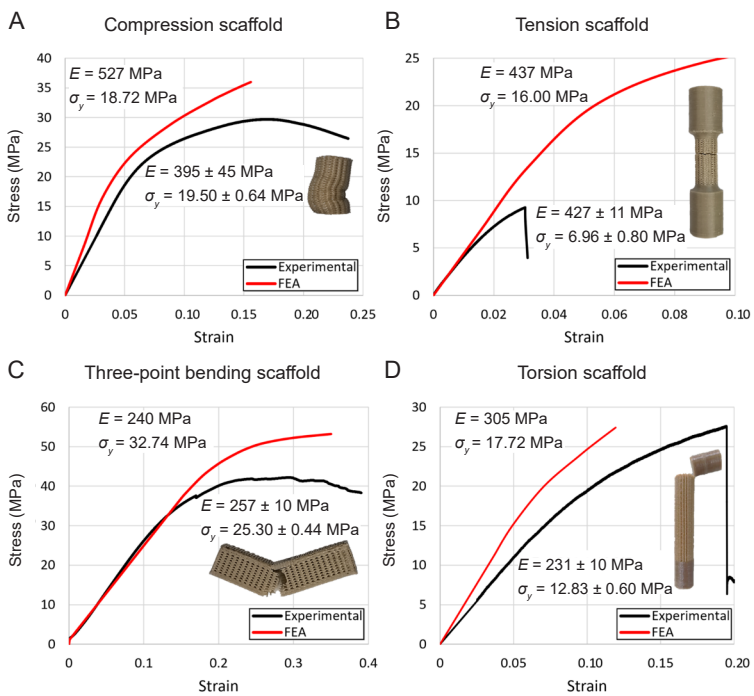

Figure 6. (A–D) Stress-strain curve of experimental and finite element model in compression (A), tension (B) and three-point bending (C), and torsion (D) scaffolds. *E*: Modulus; FEA: finite element analysis; *G*: shear modulus; σ_y: yield strength.

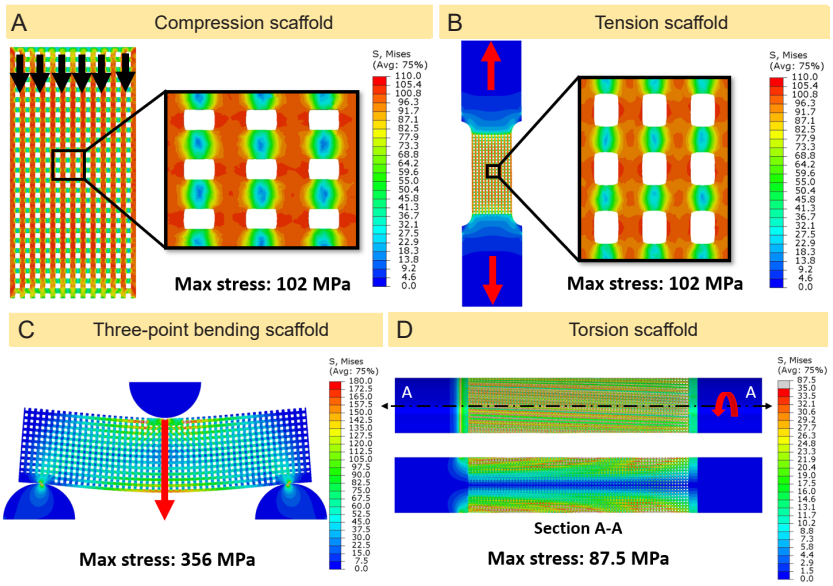

Figure 7. (A–D) Section view of finite element model results of compression (A) tension (B), three-point bending (C), and torsion (D) scaffolds. The red arrows show the direction of the applied load.

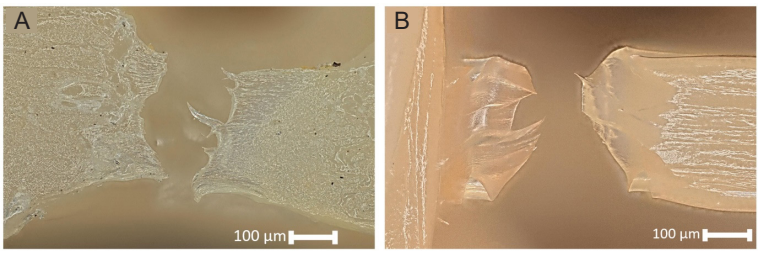

Figure 8. (A, B) Digital microscope images of the cracked tensile (A) and bending (B) scaffolds. Scale bars: 100 µm.

Table 3. Comparison of mechanical properties obtained from the experimental data, finite element plasticity model from compression, tension, three-point bending and torsion testing

Test	Young's modulus (MPa)			Yield stress (MPa)		
	Experimental	Simulation	% Error	Experimental	Simulation	% Error
Compression	395±45	527	25.1	19.50±0.64	18.72	4.2
Tension	427±11	437	2.4	6.96±0.80	16.00	56.5
Three-point bending	257±10	240	7.1	25.30±0.44	32.74	22.7
Torsion	231±10	305	24.4	12.83±0.60	17.72	27.6

the FFF process and none of the samples was subjected to heat treatment, which resulted in a lower crystallinity. The lower crystallinity gave the PEEK specimens high toughness.[25] In compression, tension and bending tests, where the failure mode in bending was also essentially some of the micro-rods of the specimens subjected to tensile strain, both showed significant toughness. However, the torque-rotation curves in the torsion test suggested a very different failure mode, with specimens breaking at very small torsion angles. The torsion specimens were printed with their axis perpendicular to the build platform, and the shear failure occurred at the interface between layers during the torsion experiment. The brittle fracture of the torsional specimens exposed the lack of interlayer bonding strength presented in FFF, which needs to be critically considered in the clinical applications.

Discussion

Difference between theoretic and actual strength

Simulated stress-strain curves for the rectilinear scaffolds for compression, tension and three-point bending test were compared with their respective experimental data in **Figure 6**. Overall, we can see a good consistency in the compression data for all samples with a smooth transition from elastic to plastic region. The general trend which can be seen in almost all data is that the FEA results overestimate Young's modulus and yield strength values compared to experimental measurements, except yield strength of FE compression and Young's modulus of FE bending which were lower than the experimental results. This overestimation can be explained by the material and manufacturing defects which creates imperfect geometry compared to the designed model. With filament 3D printing,

there will always be a small gap between the outer edge of any two overlaying layers (clearly shown in **Figure 3C**) which can act as stress concentrators and initiate crack. Hence, this would result in a lower Young's modulus and yield strength of the printed scaffold. It is also clear that the compressive, tensile and bending Young's modulus and yield strength of the scaffolds are less than those of the bulk Ti6Al4V. The results in **Table 3** demonstrate Young's modulus, yield strength and percentage error between the experimental and FEA results for all tested scaffolds in compression, tension, three-point bending and torsion. The good consistency demonstrated by the FEA in this study may be attributed to the accurate mechanical properties in the FEA model, which was obtained from the measurement of the bulk PEEK specimens manufactured by the same AM technology and printing parameters. The FEA approach in this study provides a viable method for predicting the mechanical properties of PEEK porous structure for different designed porosity and unit cells, and will enable a database of mechanical properties and porous structure of PEEK materials to be built up through computational simulation rather than through costly and time consuming experiments.

Actual strength *vs.* clinical requirement

Overall, the compressive, tensile and bending modulus of porous structures in this investigation with theoretical porosity of 50% and measured porosity of 61% reduced to 16.2–27.0% of bulk PEEK made by the same AM technology, while the yield strength decreased to 11.6–42.2% of that of bulk PEEK. The trend of the mechanical properties was largely consistent with Gibson-Ashby model. For comparison, the elastic modulus of the cancellous bone of human body ranges from 100–1000 MPa, which was comparable to that of porous AM PEEK, which would be conducive to stress stimulation of the bone tissue growing into the space of porous structure.[26] However, the low yield strength of the porous AM PEEK makes it difficult to be used as a long-bearing implant. For example, the AM PEEK mandible implant without porous structure was subjected to a maximum von Mises stress of 38 MPa.[10] As for AM PEEK porous implant, although none of them have been used in clinics, a maximum stress of 91 MPa was reported in an FEA study of porous PEEK for cranial repair when the porous PEEK cranial patch was subjected to a load of 608 N,[27] close to the yield strength of the PEEK material. Therefore, in the design of PEEK orthopaedic implant incorporating porous structures, the distribution of porous region must be carefully considered to avoid their load-bearing, which posed a challenge for both the design and AM of PEEK orthopaedic implant, as this requirement will allow the common implant with homogeneous structure evolve into non-homogeneous structures. The clinical requirements beyond the mechanical properties, biocompatibility and radiolucency of bulk PEEK, but also the conflict between the osseointegration of porous PEEK and its reduction of mechanical properties would be taken into account in the design and AM of future PEEK orthopaedic implants. Gradient porous design methodology,[28] a technique that has been extensively investigated in the AM metal porous implant,[29, 30] will likely be used to resolve the conflict. The relationship between anisotropy presented in the AM processes and the mechanical performance of the AM implant has not been studied in depth till now. Usually, all the AM technologies suffer from anisotropy due to the layer-by-layer forming principle, and it is particularly pronounced in FFF. In the present study, the torsional specimens were damaged precisely due to the weakness of the layers. This raised a cautionary note for AM implants that anisotropy must be carefully incorporated in design and fabrication.

Conclusions and prospects

In this study, mechanical tests, FEA and morphological examinations were employed to systematically investigate the mechanical properties and failure modes of AM PEEK porous structure under four loading patterns. The FEA predicted elastic modulus and yield stress, which was in good consistency with experimental data and proved to be potential as a method for rapidly establishing a database of PEEK porous structures and their mechanical properties. The mechanical properties of the PEEK porous structure specimens designed with 50% porosity were in a similar range of cancellous bone of human body, and all the PEEK specimens exhibited ductile fracture modes under different loading patterns. This study provides support for the mechanical aspects of clinical translation of AM PEEK orthopaedic implant. The porous structure is beneficial for improving osseointegration of PEEK implant, but the weak mechanical properties present a challenge for the design and AM. It will be recommendable to carry out fatigue tests and *in vivo* studies to examine the long-term endurance of PEEK porous structures.

Author contributions

Conceptualization, and methodology: SAN, CS; data curation: SAN, MH; investigation, formal analysis, validation, and manuscript draft: SAN; supervision: MM, LW, CL; manuscript revision: SAN, CS, MH, MT, JZ, LW, CZ, SNV, DL, MM, LW, CL. All authors approved the final version of this manuscript.

Financial support

The study was financially supported by National Key R&D Program of China (No. 2018YFE0207900); Natural Science Basic Research Program of ShaanXi Province (No. 2022JQ-378); The EU via the H2020-MSCA-RISE-2016 Program (No. 734156); Engineering and Physical Sciences Research Council via DTP CASE Programme (No. EP/T517793/1); and Royal Society via an International Exchange Program (No. IEC\NSFC\191253).

Acknowledgement

The authors wish to express their gratitude to Juan Leal and Mark Harrison (University College London, UK) for their technical support on mechanical testing machines.

Conflicts of interest statement

The authors declare that they have no conflicts of interests or personal relationships that could have appeared to influence the work reported in this paper.

Editor note: Chaozong Liu is an Editorial Board member of *Biomaterials Translational*. He was blinded from reviewing or making decisions on the manuscript. The article was subject to the journal's standard procedures, with peer review handled independently of this Editorial Board member and his research group.

1. Verma, S.; Sharma, N.; Kango, S.; Sharma, S. Developments of PEEK (Polyetheretherketone) as a biomedical material: a focused review. *Eur Polym J.* **2021**, *147*, 110295.
2. Yu, Y. H.; Liu, S. J. Polyetheretherketone for orthopedic applications: a review. *Curr Opin Chem Eng.* **2021**, *32*, 100687.
3. Gu, X.; Sun, X.; Sun, Y.; Wang, J.; Liu, Y.; Yu, K.; Wang, Y.; Zhou, Y. Bioinspired modifications of PEEK implants for bone tissue engineering. *Front Bioeng Biotechnol.* **2020**, *8*, 631616.
4. Zanjanijam, A. R.; Major, I.; Lyons, J. G.; Lafont, U.; Devine, D. M. Fused filament fabrication of PEEK: a review of process-structure-property relationships. *Polymers.* **2020**, *12*, 1665.
5. Kurtz, S. M.; Devine, J. N. PEEK biomaterials in trauma, orthopedic, and spinal implants. *Biomaterials.* **2007**, *28*, 4845-4869.
6. Liu, C. Z.; Sachlos, E.; Wahl, D. A.; Han, Z. W.; Czernuszka, J. T. On the manufacturability of scaffold mould using a 3D printing technology. *Rapid Prototyp J.* **2007**, *13*, 163-174.
7. Alemán-Domínguez, M. E.; Giusto, E.; Ortega, Z.; Tamaddon, M.; Benítez, A. N.; Liu, C. Three-dimensional printed polycaprolactone-microcrystalline cellulose scaffolds. *J Biomed Mater Res B Appl Biomater.* **2019**, *107*, 521-528.
8. Kang, J.; Wang, L.; Yang, C.; Wang, L.; Yi, C.; He, J.; Li, D. Custom design and biomechanical analysis of 3D-printed PEEK rib prostheses. *Biomech Model Mechanobiol.* **2018**, *17*, 1083-1092.
9. Wang, L.; Huang, L.; Li, X.; Zhong, D.; Li, D.; Cao, T.; Yang, S.; Yan, X.; Zhao, J.; He, J.; Cao, Y.; Wang, L. Three-dimensional printing PEEK implant: a novel choice for the reconstruction of chest wall defect. *Ann Thorac Surg.* **2019**, *107*, 921-928.
10. Kang, J.; Zhang, J.; Zheng, J.; Wang, L.; Li, D.; Liu, S. 3D-printed PEEK implant for mandibular defects repair - a new method. *J Mech Behav Biomed Mater.* **2021**, *116*, 104335.
11. Liu, D.; Fu, J.; Fan, H.; Li, D.; Dong, E.; Xiao, X.; Wang, L.; Guo, Z. Application of 3D-printed PEEK scapula prosthesis in the treatment of scapular benign fibrous histiocytoma: A case report. *J Bone Oncol.* **2018**, *12*, 78-82.
12. Sun, F.; Shen, X.; Zhou, N.; Gao, Y.; Guo, Y.; Yang, X.; Wu, G. A speech bulb prosthesis for a soft palate defect with a polyetherketoneketone (PEKK) framework fabricated by multiple digital techniques: a clinical report. *J Prosthet Dent.* **2020**, *124*, 495-499.
13. Wu, C.; Zeng, B.; Deng, J.; Shen, D.; Wang, X.; Tan, L.; Liu, X.; Qiu, G. Custom design and biomechanical clinical trials of 3D-printed polyether ether ketone femoral shaft prosthesis. *J Biomed Mater Res B Appl Biomater.* **2022**. doi: 10.1002/jbm.b.35055.
14. Najeeb, S.; Bds, Z. K.; Bds, S. Z.; Bds, M. S. Bioactivity and osseointegration of PEEK are inferior to those of titanium: a systematic review. *J Oral Implantol.* **2016**, *42*, 512-516.
15. Walsh, W. R.; Pelletier, M. H.; Bertollo, N.; Christou, C.; Tan, C. Does PEEK/HA enhance bone formation compared with PEEK in a sheep cervical fusion model? *Clin Orthop Relat Res.* **2016**, *474*, 2364-2372.
16. Zheng, J.; Zhao, H.; Ouyang, Z.; Zhou, X.; Kang, J.; Yang, C.; Sun, C.; Xiong, M.; Fu, M.; Jin, D.; Wang, L.; Li, D.; Li, Q. Additively-manufactured PEEK/HA porous scaffolds with excellent osteogenesis for bone tissue repairing. *Compos B Eng.* **2022**, *232*, 109508.
17. Zhu, Y.; Cao, Z.; Peng, Y.; Hu, L.; Guney, T.; Tang, B. Facile surface modification method for synergistically enhancing the biocompatibility and bioactivity of poly(ether ether ketone) that induced osteodifferentiation. *ACS Appl Mater Interfaces.* **2019**, *11*, 27503-27511.
18. Zheng, J.; Zhao, H.; Dong, E.; Kang, J.; Liu, C.; Sun, C.; Li, D.; Wang, L. Additively-manufactured PEEK/HA porous scaffolds with highly-controllable mechanical properties and excellent biocompatibility. *Mater Sci Eng C Mater Biol Appl.* **2021**, *128*, 112333.
19. Oladapo, B. I.; Ismail, S. O.; Adebiyi, A. V.; Omigbodun, F. T.; Olawumi, M. A.; Olawade, D. B. Nanostructural interface and strength of polymer composite scaffolds applied to intervertebral bone. *Colloids Surf Physicochem Eng Aspects.* **2021**, *627*, 127190.
20. Zhong, G.; Vaezi, M.; Mei, X.; Liu, P.; Yang, S. Strategy for controlling the properties of bioactive poly-ether-ether-ketone/hydroxyapatite composites for bone tissue engineering scaffolds. *ACS Omega.* **2019**, *4*, 19238-19245.
21. Seo, J.; Gohn, A. M.; Dubin, O.; Takahashi, H.; Hasegawa, H.; Sato, R.; Rhoades, A. M.; Schaake, R. P.; Colby, R. H. Isothermal crystallization of poly(ether ether ketone) with different molecular weights over a wide temperature range. *Polym Cryst.* **2019**, *2*, e10055.
22. International Organization for Standardization. ISO 13314:2011. Mechanical testing of metals — ductility testing — compression test for porous and cellular metals.
23. American National Standards Institute. ASTM E143-13. Standard test method for shear modulus at room temperature.
24. Maskery, I.; Sturm, L.; Aremu, A. O.; Panesar, A.; Williams, C. B.; Tuck, C. J.; Wildman, R. D.; Ashcroft, I. A.; Hague, R. J. M. Insights into the mechanical properties of several triply periodic minimal surface lattice structures made by polymer additive manufacturing. *Polymer.* **2018**, *152*, 62-71.
25. Yang, C.; Tian, X.; Li, D.; Cao, Y.; Zhao, F.; Shi, C. Influence of thermal processing conditions in 3D printing on the crystallinity and mechanical properties of PEEK material. *J Mater Process Technol.* **2017**, *248*, 1-7.
26. Carpenter, R. D.; Klosterhoff, B. S.; Torstrick, F. B.; Foley, K. T.; Burkus, J. K.; Lee, C. S. D.; Gall, K.; Guldberg, R. E.; Safranski, D. L. Effect of porous orthopaedic implant material and structure on load sharing with simulated bone ingrowth: A finite element analysis comparing titanium and PEEK. *J Mech Behav Biomed Mater.* **2018**, *80*, 68-76.
27. El Halabi, F.; Rodriguez, J. F.; Rebolledo, L.; Hurtós, E.; Doblaré, M. Mechanical characterization and numerical simulation of polyether-ether-ketone (PEEK) cranial implants. *J Mech Behav Biomed Mater.* **2011**, *4*, 1819-1832.
28. Sun, C.; Wang, L.; Kang, J.; Li, D.; Jin, Z. Biomechanical optimization of elastic modulus distribution in porous femoral stem for artificial hip joints. *J Bionic Eng.* **2018**, *15*, 693-702.
29. Jiang, Q.; Zaïri, F.; Fréderix, C.; Yan, Z.; Derrouiche, A.; Qu, Z.; Liu, X.; Zaïri, F. Biomechanical response of a novel intervertebral disc prosthesis using functionally graded polymers: A finite element study. *J Mech Behav Biomed Mater.* **2019**, *94*, 288-297.
30. Sola, A.; Bellucci, D.; Cannillo, V. Functionally graded materials for orthopedic applications - an update on design and manufacturing. *Biotechnol Adv.* **2016**, *34*, 504-531.

Received: May 4, 2022
Revised: June 2, 2022
Accepted: June 9, 2022
Available online: June 28, 2022